Infrared Linear Tapered Slot Antenna

Louis A. Florence, Brian A. Slovick, *Member, IEEE*, Edward C. Kinzel, Jeffrey A. Bean, *Member, IEEE*, and Glenn D. Boreman, *Senior Member, IEEE*

***Abstract*—For the first time, a tapered slot antenna coupled to a metal–oxide–metal (MOM) diode is designed, fabricated, and characterized at an infrared wavelength of 10.6 μm. Polarization ratio was measured to be approximately 6.7:1. The antenna's radiation pattern shows beamwidth symmetry between the E-plane and the H-plane data, having full width at half-maximum beamwidths of 45° and 30°, respectively.**

***Index Terms*—Antenna radiation pattern, infrared detector, thin film devices.**

I. Introduction

INFRARED antennas have historically been limited by their detector elements. Fast, small bolometers tend to be low-response devices, requiring high field concentrations for dependable results [1]. Therefore, only planar antennas such as dipoles, spirals, bowties, and log-periodics have been incorporated into antenna-coupled sensor devices [2]. With the recent developments in IR microdiodes [3], traveling-wave antenna designs with desirable characteristics such as endfire operation and very wide bandwidth are now feasible.

Tapered slot antennas (TSAs) [4]–[6] offer several desirable capabilities for detection of infrared radiation over existing microstrip antenna coupled detectors. TSAs are endfire planar antennas that begin with a several-wavelengths-wide aperture cut into the edge of a metal sheet and gradually narrowed into a wave-guiding slot. The endfire operation and low-profile planar geometry offer a degree of integration flexibility unavailable to non-endfire antennas, such as multilayer stacking. These antennas have been shown experimentally[1] to have both a multioctave bandwidth because they are nonresonant and an impedance that does not change drastically along the antenna [7]. Instead, radiation is gradually confined into the slot by the metal surfaces. Potential applications of these devices include infrared detection, directional signal transmission and reception, and energy harvesting.

Manuscript received September 09, 2011; revised October 18, 2011; accepted November 04, 2011. Date of publication November 21, 2011; date of current version December 05, 2011.

L. A. Florence is with the Center for Research and Education in Optics and Lasers (CREOL), The College of Optics and Photonics, University of Central Florida, Orlando, FL 32816 USA (e-mail: Louis.florence@knights.ucf.edu).

B. A. Slovick is with SRI International, Menlo Park, CA 94025 USA.

E. C. Kinzel is with the Department of Physics and Optical Science, University of North Carolina at Charlotte, Charlotte, NC 28146 USA.

J. A. Bean is with Georgia Tech Research Institute, Atlanta, GA 30332 USA.

G. D. Boreman is with the Department of Physics and Optical Science, University of North Carolina at Charlotte, Charlotte, NC 28146 USA, and also with the Center for Research and Education in Optics and Lasers (CREOL), The College of Optics and Photonics, University of Central Florida, Orlando, FL 32816 USA.

Color versions of one or more of the figures in this letter are available online at http://ieeexplore.ieee.org.

Digital Object Identifier 10.1109/LAWP.2011.2176904

[1]Gibson [4] reported a two-octave (8–40 GHz) device.

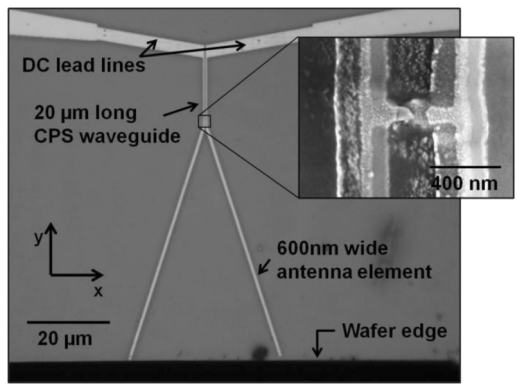

Fig. 1. Top view of the device as built with an expanded view of the diode. The bright smooth metal is platinum, while the darker coarse metal is aluminum.

In this letter, we discuss the design, fabrication and characterization of a V-shaped linear TSA (V-LTSA) coupled to a zero-bias metal–oxide–metal (MOM) tunnel diode operating at 28.3 THz (10.6 μm). The thin metal antenna arms and slotlines of the V-LTSA are expected to suppress surface-wave and parallel-plate modes common in TSAs with large metal sheets, and thus increase the strength of the mode in the slotline [8]. Measured polarization dependence and radiation patterns demonstrate the desirable aspects of this class of antennas at infrared frequencies.

II. Antenna Design

The scaling of operational antennas from microwave to infrared frequencies presents a variety of challenges. The resonant dimensions of the infrared antenna elements and diodes are submicron and require resolution beyond the capabilities of traditional photolithography, so electron-beam lithography is necessary. Also, the unique material properties of dielectrics and metals in this band must be considered. Few low-loss substrate materials exist in the thermal infrared due to molecular vibrational states [9]. Additionally, metals are known to have significant dispersion and loss in the infrared that reduce antenna performance [10]. These loss mechanisms greatly reduce the propagation length of the infrared radiation in the V-LTSA, reducing the gain of the antenna. Fabrication of the MOM tunnel diode adds additional constraints. We use a shadow evaporation technique [11] that typically sets the minimum dimensions that can be fabricated.

The top view of the antenna-coupled detector is shown in Fig. 1. The endfire V-LTSA is placed with its opening at the cleaved edge of a silicon wafer. The insulating substrate is 1.6 μm of benzo-cyclobutane (BCB), chosen for its low

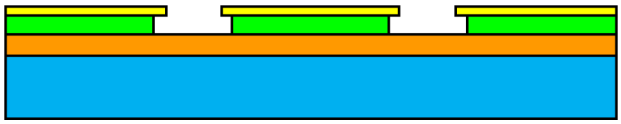

Fig. 2. Not-to-scale front view of the resist and substrate layers shown after lithography and development. The bottom layer is the silicon wafer, covered with a layer of BCB. The second layer (MMA) from the top is more sensitive than the top layer (PMMA), allowing the tunnel diode to be created by the shadow evaporation technique.

index $(\mathrm{n} = 1.52)$ and low loss $(\mathrm{k} = 0.02)$ at 28.3 THz. Lead lines are present to measure the dc current generated by the rectifying diode. Optimization of the design was accomplished using commercially available finite-element analysis software, Ansoft's High Frequency Structure Simulator (HFSS). The length of the taper is 60 μm, the end taper width is 40 μm, and the feed into the coplanar stripline (CPS) is 0.4 μm wide. The metal trace lines forming the antenna are 0.6 μm wide, while the metal lines forming the CPS are 0.2 μm wide.

The CPS is 20 μm long, with the diode placed inside the CPS 1.5 μm from the taper. The design of the CPS was chosen to simulate a feeding CPS while keeping the dc feed lines far from the diode. The metal sections forming the structure are misaligned by the shadow evaporation technique required to make the MOM tunnel diode. The metal thickness of both the model and the actual device are 30 nm of aluminum, with 2 nm of native aluminum oxide, capped with 30 nm of platinum. The aluminum is deposited with positive angular offset from the substrate's normal; the platinum is deposited with a negative angular offset. This allows a 90×90 nm^2 MOM diode to be formed in the center of the CPS, but also causes a 120-nm misalignment of the two metals.

III. Antenna Fabrication and Measurement

The antenna was fabricated on a 375-μm-thick silicon wafer. Onto the wafer, 1.6 μm of BCB was spin-coated and cured in a nitrogen environment at 250°C. The antenna pattern was written using a Leica EBPG 5000+ Electron Beam Lithographer into a bilayer resist stack of 500 nm of MMA capped with 50 nm PMMA (Fig. 2). The wafer, BCB, and resist are cleaved to provide a straight edge, and the pattern is written across a cleaved edge of the wafer, thus ensuring endfire operation.

Once the resist is developed, the wafer is mounted on a custom adjustable stage inside an ultrahigh vacuum electron beam evaporator. The tilt stage allows metals to be deposited at positive and negative angles without removing the sample from vacuum. Initially, 30 nm of aluminum are deposited at $+7°$. Next, 80 mTorr of pure oxygen are bled into the chamber to allow for controlled oxide layer growth for 30 min, resulting in approximately 2 nm of aluminum oxide covering the aluminum surfaces. Then, the stage is tilted *in situ* to an opposing negative angle, and 30 nm of platinum are deposited.

After lifting off the unwanted metals and resist, the device is electrically connected to a five-axis goiniometer stage, allowing the device to be centered about the stage's axes of rotation and then rotated in both azimuth and elevation [12]. The test source is a CO_2 laser operating at a wavelength of 10.6 μm (28.3 THz). The signal's polarization is controlled by a wire grid polarizer and a half-wave plate. A pick-off integrated in the optical train of the laser provides a power reference so that the measurement will not be influenced by fluctuations in laser power. A chopper is used to modulate the signal at 1420 Hz to verify the rapid response of the detector and avoid 1/f and 60-Hz noise. The beam from the laser is focused to a spot with an e^{-2} radius of 115 μm. During alignment, the phase center of the antenna is placed in the center of this spot. The antenna's dc current response is amplified by a low-noise $10\times$ amplifier and recorded by a lock-in amplifier synchronized to the chopper frequency. This current response is normalized to the reference power and recorded. The E- and H-plane patterns are generated by varying the azimuth and elevation of the antenna while keeping the laser beam fixed.

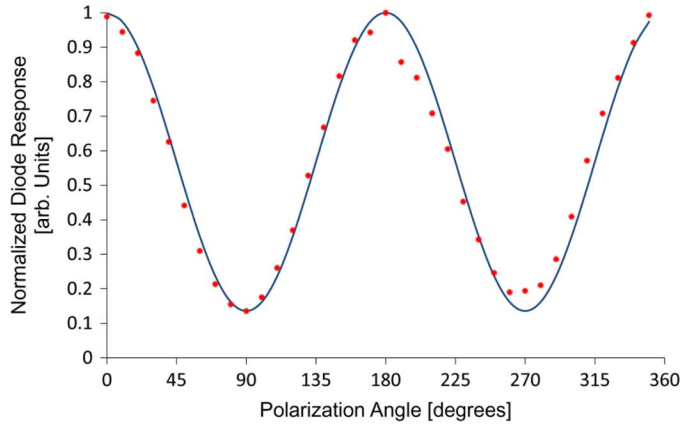

Fig. 3. Polarization data points and a cosine-squared curve showing the polarization dependence for this antenna. Data was taken with the device centered at broadside.

TSAs responses are polarization-dependent. We varied the polarization of the laser by rotating a half-wave plate and measured the response of the TSA (Fig. 3). By fitting the data with a $\cos^2(\theta)$ curve, we deduce that the antenna is operating as expected and rule out thermal or photovoltaic effects, as these effects would produce signal independent of polarization. The cross-polarized signal is 15% of the copolarized signal for a 6.7:1 polarization ratio.

To model the radiation pattern of the antenna in receiving mode, a transmitting model of the antenna is built in HFSS. A waveport in HFSS excites a mode in the CPS at 10.6 μm (28.3 THz). This excited mode is then propagated through the volume of the model to the outer surfaces. Knowing the field distribution at the outer surfaces of the model allows the calculation of the far-field radiation pattern for the transmitting antenna. From reciprocity, the radiation pattern of the transmitting model and the receiving antenna are equivalent. This far-field radiation pattern is used as the expected antenna response.

As shown in Fig. 4(a) and (b), the experimental results are in good agreement with the HFSS simulations. The beam patterns show an H-plane (the yz-plane as shown in Fig. 1) half-maximum beamwidth of 30°. The E-plane (the xy-plane from Fig. 1) radiation pattern represents the device being held at a constant elevation of $-30°$ (i.e., where the H-plane experiences its maximum). Its half-maximum beamwidth is 45°. Previous work in the millimeter-wave regime achieved near-perfect symmetry and true endfire operation in both planes because materials for

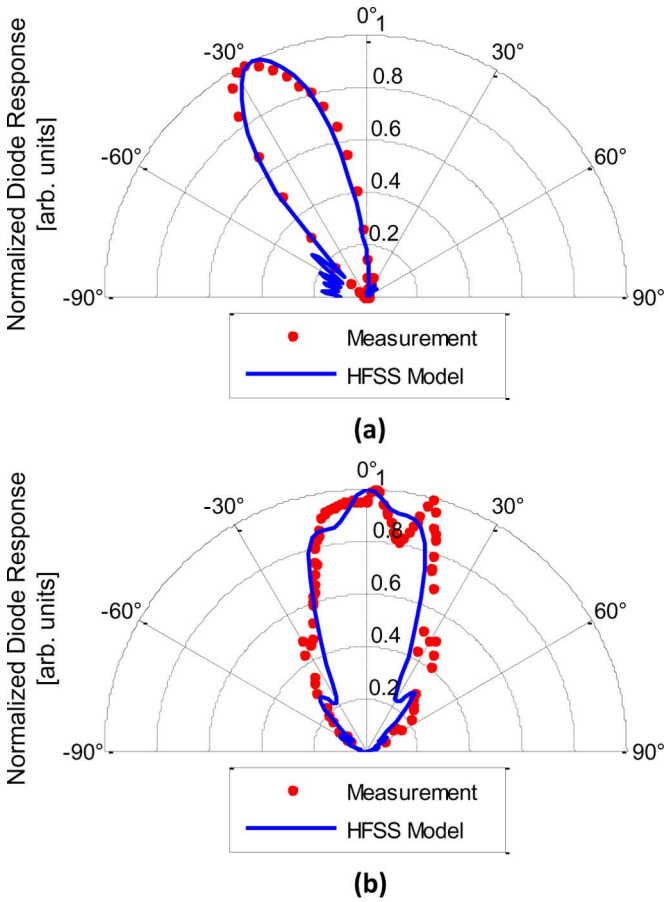

Fig. 4. Modeled (solid line) and measured radiation pattern normalized data points. (a) The H-plane (yz-plane from Fig. 1) pattern shows a maximum at $-30°$, while (b) the E-plane pattern (xy-plane rotated to $-30°$) is nearly symmetric about the endfire direction.

the substrate and the superstrate possessed similar indices of refraction, such as air and Styrofoam [13]. The $-30°$ offset of the H-plane patter is caused by an index mismatch between the air superstrate and the BCB/silicon wafer substrate. HFSS predicts that if the superstrate and the substrate are the same material, the infrared antennas will operate in a true endfire-symmetric pattern.

The device's peak response was approximately 8 nA/(W/cm^2). This low responsivity is a result of several loss mechanisms in the substrate and the antenna, impedance mismatches, and the limited nonlinearity of the diode. Future improvements proposed in the diode design and substrate stand to greatly enhance this responsivity.

One promising solution to the responsivity problem is the use of a superstrate, or immersing the antenna into a medium with the same index as the standoff layer. Not only would the superstrate improve the symmetry of the H-plane about the endfire direction, but HFSS simulations suggest it will raise the responsivity by an order of magnitude because of increased confinement. The effects of this superstrate on the diode have not been explicitly studied, but the expected increase in responsivity could make the V-LTSA coupled with a tunnel diode a viable solution for broadband IR detection.

IV. Conclusion

We have constructed an endfire V-LTSA capable of detecting infrared radiation. The antenna has a well-defined beam profile with sidelobes of less than 50% of the maximum signal. The antenna has a beamwidth nearly symmetric in the E- and H-planes.

Further study is needed to understand the effects of the various design parameters to include physical dimensions, choice of substrate, and use of a superstrate for increased responsivity. Also, the advantages and disadvantages of other shapes known to the microwave community (linear TSA, exponential TSA, double exponential TSA, etc.) [14] can now be modeled, fabricated, and studied at infrared frequencies. With these advances, we expect that the infrared VTSA coupled with a tunnel diode will become a desirable sensor for broadband IR detection.

References

[1] E. Dereniak and G. Boreman, *Infrared Detectors and Systems*. New York: Wiley, 1996, p. 413.
[2] F. Gonzalez and G. Boreman, "Comparison of dipole, bowtie, spiral and log-periodic IR antennas," *Infrared Phys. Technol.*, vol. 46, no. 5, pp. 418–428, Jun. 2005.
[3] J. Bean, A. Weeks, and G. Boreman, "Performance optimization of antenna-coupled Al/AlOX/Pt tunnel diode infrared detectors," *IEEE J. Quantum Electron.*, vol. 47, no. 1, pp. 126–135, Jan. 2011.
[4] P. J. Gibson, "The Vivaldi aerial," in *Proc. 9th Eur. Microw. Conf.*, Brighton, U.K., 1979, pp. 101–105.
[5] K. Yngvesson, T. Korzeniowski, Y. Kim, E. Kollberg, and J. Johansson, "The tapered slot antenna—A new integrated element for millimeter wave applications," *IEEE Trans. Microw. Theory Tech.*, vol. 37, no. 2, pp. 365–374, Feb. 1989.
[6] T. Hwang, D. Rutledge, and S. Schwarz, "Planar sandwich antennas for submillimeter applications," *Appl. Phys. Lett.*, vol. 34, no. 1, pp. 9–11, Jan. 1979.
[7] R. Janaswamy and D. Schaubert, "Analysis of the tapered slot antenna," *IEEE Trans. Antennas Propag.*, vol. AP-35, no. 9, pp. 1058–1065, Sep. 1987.
[8] J. J. Lee and S. Livingston, "Wide band bunny-ear radiating element," in *Proc. IEEE Antennas Propag. Soc. Int. Symp.*, Ann Arbor, MI, Jul. 1993, pp. 1604–1607.
[9] M. Fox, *Optical Properties of Solids*, 2nd ed. Oxford, U.K.: Oxford Univ. Press, 2010, p. 216.
[10] F. Gonzalez, J. Alda, J. Simon, J. Ginn, and G. Boreman, "The effect of metal dispersion on the resonance of antennas at infrared frequencies," *Infrared Phys. Technol.*, vol. 52, no. 1, Jan. 2009.
[11] J. A. Bean, B. Tiwari, G. H. Bernstein, P. Fay, and W. Porod, "Thermal infrared detection using dipole antenna-coupled metal-oxide-metal diodes," *J. Vac. Sci. Technol. B*, vol. 27, no. 1, pp. 11–14, 2009.
[12] P. Krenz, B. Slovick, J. Bean, and G. Boreman, "Alignment procedures for radiation pattern measurements of antenna-coupled infrared detectors," *Opt. Eng.*, vol. 49, no. 4, pp. 033607-1–033607-5, 2010.
[13] K. Yngvesson, D. Schaubert, T. Korzeniowski, E. Kollberg, T. Thungren, and J. Johansson, "Endfire tapered slot antennas on dielectric substrates," *IEEE Trans. Antennas Propag.*, vol. AP-33, no. 12, pp. 1392–1400, Dec. 1985.
[14] R. Lee and R. N. Simons, , K. F. Lee and W. Chen, Eds., "Tapered Slot Antennas," in *Advances in Microstrip and Printed Antennas*. New York: Wiley, 1997, pp. 443–514.